中国光学（中英文） Chinese Optics 核心期刊

Laser processing of flexible and stretchable RGO in-plane micro-supercapacitors with strong performance robustness

JIANG Hao-bo, ZHANG Yu-yin, ZHANG Yu-yuan, WANG Zhe, FU Xiu-yan, LI Hua-rui, LIU Jian-qi, XIN Wei

Citation:
JIANG Hao-bo, ZHANG Yu-yin, ZHANG Yu-yuan, WANG Zhe, FU Xiu-yan, LI Hua-rui, LIU Jian-qi, XIN Wei. Laser processing of flexible and stretchable RGO in-plane micro-supercapacitors with strong performance robustness[J]. *Chinese Optics*, In press. doi: 10.3724/CO.EN-2026-0011
姜昊伯, 张誉尹, 张誉元, 王哲, 付秀燕, 李骅芮, 刘健琦, 辛巍. 高鲁棒RGO柔性可拉伸平面微型超级电容器的激光制造与性能研究[J]. 中国光学, 优先发表. doi: 10.3724/CO.EN-2026-0011

View online: https://doi.org/10.3724/CO.EN-2026-0011

Articles you may be interested in

Fully complex optical neural network with insertion-loss robustness
插损鲁棒性的全复值光学神经网络
Chinese Optics. 2024, 17(4): 834 https://doi.org/10.37188/CO.2023-0198

Vibration sensor based on stretchable optical fiber and interferometric measurement
基于可拉伸光纤和干涉测量的振动传感器
Chinese Optics. 2025, 18(5): 1200 https://doi.org/10.37188/CO.EN-2025-0010

High anti-icing performance of coating-free superhydrophobic metal surfaces via femtosecond laser processing
具有高防冰性能的飞秒激光加工无涂层超疏水金属表面
Chinese Optics. 2025, 18(6): 1506 https://doi.org/10.37188/CO.EN-2025-0013

Angle-multiplexed optically encrypted metasurfaces fabricated by ultrafast laser induced spatially selective-modified nanograting structures
角度复用的光学加密超表面的超快激光嵌套加工方法研究
Chinese Optics. 2023, 16(4): 889 https://doi.org/10.37188/CO.2022-0228

Laser-assisted water jet machining of high quality micro-trap structures on stainless steel surfaces
不锈钢表面高质量微陷阱结构的激光辅助水射流加工
Chinese Optics. 2024, 17(6): 1476 https://doi.org/10.37188/CO.EN-2024-0004

Multi-robot collaborative optical processing
多机器人协同光学加工技术
Chinese Optics. 2025, 18(6): 1353 https://doi.org/10.37188/CO.2025-0020

文章编号　2097-1842(xxxx)x-0001-13

Laser processing of flexible and stretchable RGO in-plane micro-supercapacitors with strong performance robustness

JIANG Hao-bo[1*], ZHANG Yu-yin[1,3], ZHANG Yu-yuan[2], WANG Zhe[2], FU Xiu-yan[1*], LI Hua-rui[1], LIU Jian-qi[1], XIN Wei[2*]

(1. *Key Laboratory of Functional Materials Physics and Chemistry of Ministry of Education*, *College of Physics*, *Jilin Normal University*, *Changchun* 130103, *China*;
2. *State Key Laboratory of Integrated Optoelectronics*, *Key Laboratory of UV-Emitting Materials and Technology of Ministry of Education*, *Northeast Normal University*, *Changchun* 130024, *China*;
3. *Changchun Technical University of Automobile*, *Changchun* 130103, *China*)

* *Corresponding author*, *E-mail*: *jianghaobo@jlnu.edu.cn*; *fuxy@jlnu.edu.cn*; *xinwei@nenu.edu.cn*

Abstract: The performance instability and degradation of flexible and stretchable in-plane micro-supercapacitors (FS-MSCs) under large deformation have limited their applications. Selecting suitable flexible electrode materials and integrating them with stretchable substrates is crucial to solve the problem, while it remains a challenge to simplify the device preparation and optimize performance. Here, we report a programmable single-wavelength laser processing strategy that simultaneously reduces/patterns reduced graphene oxide (RGO) interdigital electrodes and textures an elastomeric substrate. By pre-stretching the substrate and fitting it to the flexible RGO electrodes, our device demonstrates excellent performance robustness. A bending angle of over 300° and a tensile strain of about 120% of its original length can be withstood. Furthermore, by optimizing the substrate surface morphology with ordered gridding, the electrochemical properties and stability of the device have been significantly improved, which achieves a maximum capacitance of 1.34 mF/cm^2 with a fluctuation of only 1.5% under different tensile conditions. Even as the current density increases from 0.01 to 0.05 mA/cm^2 gradually, the specific capacitance fluctuation of the devices remains <7.4% under varying tensile strengths. Our work offers an effective solution for enhancing performance stability of in-plane FS-MSCs in harsh deformation environments, holding great potential for their future applications in wearable and portable energy storage.

Key words: laser processing; micro-supercapacitors; RGO; robustness; flexibility and stretchability

收稿日期:2026-04-09; **修订日期**:xxxx-xx-xx

基金项目:吉林省科技发展项目(No. YDZJ202301ZYTS383);吉林省教育厅科技项目(No. JJKH20240572KJ);国家自然科学基金(No. 22478149, No. 62505109, No. 12274065);吉林师范大学博士启动基金(No. 0420104, No. 0420103)资助

Supported by the Development of Science and Technology of Jilin Province (No. YDZJ202301ZYTS383); the Science and Technology Project of Jilin Province Education Department (No. JJKH20240572KJ); the National Natural Science Foundation of China (No. 22478149, No. 62505109, No. 12274065); PhD Start-up Fund of Jilin Normal University (No. 0420104, No. 0420103)

高鲁棒 RGO 柔性可拉伸平面微型超级电容器的激光制造与性能研究

姜昊伯[1*], 张誉尹[1,3], 张誉元[2], 王　哲[2], 付秀燕[1*], 李骅芮[1], 刘健琦[1], 辛　巍[2*]
（1. 吉林师范大学 物理学院, 功能材料物理与化学教育部重点实验室, 长春 130103;
2. 东北师范大学 集成光电子学国家重点实验室, 紫外光发射材料与技术教育部重点实验室, 长春 130024;
3. 长春汽车职业技术大学, 长春 130103）

摘要: 柔性可拉伸平面微型超级电容器(FS-MSCs)在大变形下的性能不稳定和性能退化限制了其应用。选择合适的柔性电极材料并将其与可拉伸基底集成是解决该问题的关键, 但简化器件制备流程并优化性能仍面临挑战。在此, 我们报告了一种可编程的单一波长激光加工策略, 该策略可同时对氧化石墨烯(GO)叉指电极薄膜进行图案化和还原处理, 并对弹性基底规整性纹理化。通过预拉伸基底并将其与柔性电极适配, 我们的器件展现出了优异的性能鲁棒性。该器件能够承受超过 300°的弯曲角度和约为原始长度 120% 的拉伸程度。此外, 通过优化基底表面形貌至有序网格, 器件的电化学性能和稳定性得到了进一步显著提升。在不同拉伸条件下, 其最大电容达到 1.34 mF/cm^2, 波动仅为 1.5%。即使电流密度从 0.01 mA/cm^2 逐渐增加到 0.05 mA/cm^2, 在不同拉伸强度下, 器件的比电容波动仍保持在<7.4%。我们的工作为简化器件构建、并提高平面 FS-MSCs 在恶劣变形环境下的性能稳定性提供了一种有效解决方案, 在可穿戴和便携式储能的未来应用中具有巨大潜力。

关　键　词: 激光加工; 微型超级电容器; RGO; 鲁棒性; 柔性与可拉伸性
中图分类号: O482.31　　**文献标志码:** A　　**doi:** 10.3724/CO.EN-2026-0011　　**CSTR:** 32171.14.CO.EN-2026-0011

1 Introduction

Supercapacitors, as typical energy storage devices, have found widespread applications due to their superior characteristics such as high power density, fast charge/discharge rates, long-cycle life, environmental friendliness and so on [1-2]. With the rapid development of integrated optoelectronics recently, the need for flexible and stretchable micro-supercapacitors (FS-MSCs) with an optimized in-plane architecture and stable performance has been further highlighted [3-5]. In general, the performance of in-plane FS-MSCs is determined by the intrinsic properties of the electrode and substrate materials, as well as their structural integration. The former governs the electrochemical behaviors, while the latter ensures the mechanical robustness and stability [6-8]. Among various strategies that have been proposed to keep high performance of devices, attaching flexible electrodes to a pre-stretched elastomeric substrate is commonly applied [9-10]. To further optimize device performance, it is also crucial to meticulously engineer the substrates to alleviate material stress and enhance mechanical strength [11]. Micro-nano structures processed orderly and regularly can bolster the stability and controllability of devices, which is especially important in their integration into micro-chips [11-13]. However, how to fashion the structures conveniently while simplifying the overall device design is still challenging, which present significant research value to promote the development of this field.

2 Experiment

To this end, here we developed a laser direct writing technique for preparing the in-plane FS-MSCs, which consist of flexible photo-patterned reduced graphene oxide (RGO) electrodes integrated

with pre-stretched elastic substrates ablated with regular structures. The excellent mechanical properties of the selected materials ensure the devices to withstand a bending range exceeding 300° without compromising performance. Even after enduring repeat bending for 1 000 cycles, the specific capacitance remained at 111% of their initial states. The pre-stretch design of our FS-MSCs allows them to achieve a maximum stretchability of over 118%, which can adapt to most tensile demands of human skin or wearable equipment [14-15]. In addition, the specific capacitance fluctuation of our devices can be further lowered from 15.9% to 1.5% by further optimizing the structures of substrate, indicating a remarkable improvement in the stability and reliability.

It should be noted that a same light source (CO_2 laser, ~10.64 μm) was utilized for processing both the RGO electrodes and structured substrates here. We just need to functionalize the different components by controlling the parameters, which can not only improve the working efficiency but also maintain the stability of device performance during processing. Nevertheless, the CO_2 laser plays distinct roles in the above operations. In terms of electrodes, based on the thermal reduction effect, the laser can selectively eliminate oxygen-containing groups (OCGs) from graphene oxide (GO) film coated on the polymer surface, resulting in its reduced analogue [16]. By meticulously adjusting the laser parameters, this process not only maintains the high conductivity and stable physicochemical properties of the carbon materials without damages, but also enhances the specific area of RGO with hierarchical micro-nano structures, there-by promoting electrochemical reactivity in subsequent experiments [17-19]. In contrast, when it comes to the substrate, the laser can selectively ablate its surface for creating structures as design, providing convenience for controlling the performance of FS-MSCs [20-21]. While laser-processed graphene MSC, substrate structuring for mechanical robustness, and pre-stretching for enhanced flexibility/ stretchability have been reported, combining these features via a simple single-wavelength laser strategy is rarely seen [22-23]. This simplified operation, along with the control of device stress distribution through micro/nanostructures, enables the device to exhibit superior stability. The key performance metrics of our device are compared with representative works in Table 1. This work offers remarkable flexibility as it is not limited to specific materials and is compatible with existing semiconductor processes techniques, making it suitable for the widespread fabrication of integrated FS-MSCs in the future [24-25].

3 Results and Discussion

Figs. 1(a) shows the flow diagram of processing in-plane FS-MSCs using laser direct writing technique. First, GO solution was spin-coated onto the surface of a flexible polymer film, and a beam of CO_2 laser was employed to photo-reduce the GO to RGO electrodes as design [Figs. 1(a), I-II]. The GO material is selected mainly because of its excellent electrochemical performance, as well as its ease of peeling and dispersion in water, and its tractability for further electrode formation with uniform thickness [26]. Meanwhile, the interdigital structure design eliminates the need for sandwiching a membrane separator between two electrodes like traditional devices, which can greatly enhance the ion transmission efficiency, and mitigate the risks of short circuit and electrolyte leakage. Then, the laser was utilized again to ablate one-dimensional (1D) periodic grooves on an elastomeric substrate [Figs. 1 (a), IV]. A typical period of 1 mm with a 3:7 duty factor was set on an area of 2×2 cm^2. After that, the substrate was pre-stretched to 120% of its initial length, and the RGO/polymer electrode film was transferred and attached onto it to assemble them into a complete device [Figs. 1(a), III, V]. Since only the top surfaces of the grooves were in contact with the film, periodic buckling folds formed on surface

of the device as the deformation of substrate was recovered [Figs. 1(a), VI]. Finally, a PVA-H_3PO_4 gel electrolyte was drop-coated onto the interdigital RGO electrode region, filling the gaps between the fingers to form the solid-state electrolyte layer. No additional encapsulation was applied, as the gel electrolyte itself provides sufficient ionic conduction and mechanical compliance for device operation [Figs. 1(a), VII].

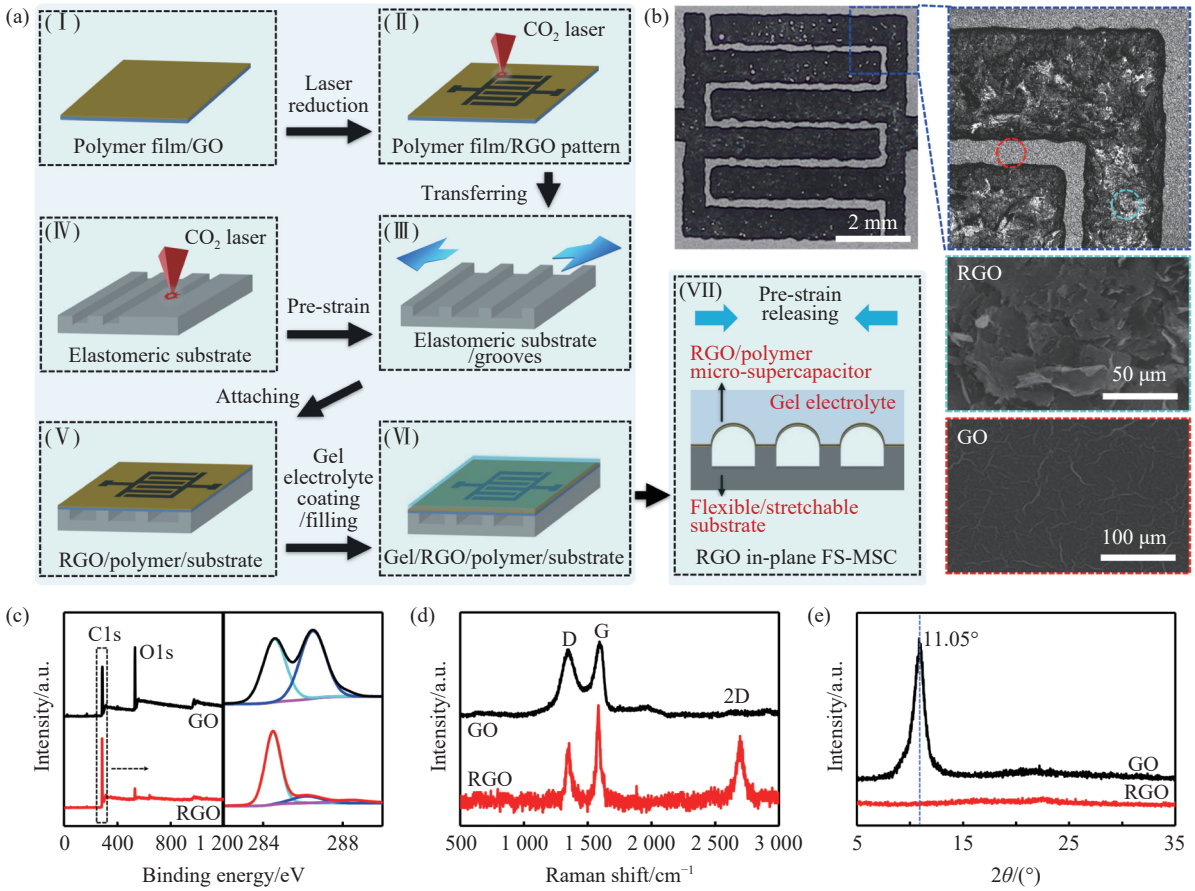

Fig. 1 (a) Schematic diagram of RGO in-plane FS-MSCs processing with laser direct writing technique. (b) OM and SEM images of local electrodes positions. (c)-(e) XPS, Raman and XRD spectra characterization of GO films where it is photo-reduced or not.

Subsequently, the morphology and chemical composition of the interdigital electrode were characterized in detail. Figs. 1b presents the optical (OM) and scanning electron microscope (SEM) images of the local electrode patterns where the GO were photo-reduced or not. The RGO area turns black obviously and the peels roll up to form plentiful hierarchical micro-nano structures. In the area of 2.6×2.6 mm^2, the fluctuation of reduced region reaches the order of 100 microns, which is beneficial to provide sufficient location for charge storage and improve electrochemical performance of the devices. Notably, our technique presents compatibility with the substrate material and offers significant flexibility in device morphology fabrication. By varying the processing conditions and parameters, different device morphologies can be achieved. Further details are available in Supplementary Information (SI) S1, S2 and S3.

To further clarify the reduction degree of GO, X-ray photoelectron spectroscopy (XPS), X-Ray Diffraction (XRD) and Raman spectra were respectively characterized. First, from the XPS results shown in Figs. 1c, two peaks at 287 and 532 eV corresponding to the C 1s and O 1s signals are seen both in GO and RGO materials, while the intensity

of O 1s peak descends obviously after reduction [27]. By fitting the C 1s spectra into three peaks, C-C, C-O and C=O components at 284.5, 286.5, 288.4 eV are obtained. Due to the laser-induced deoxygenation after treatment, the peak intensities of C-O and C=O reduce, indicating the sharp decrease of elemental oxygen content. Quantitative analysis reveals that the oxygen atomic content decreases from approximately 30.6% in GO to 8.7% in RGO, confirming effective removal of oxygen-containing functional groups (OCGs, e.g., C-OH at 285.8 eV and C-O-C at 286.7 eV). Moreover, the C-C peak of the structured RGO becomes narrower compared to that of GO, indicating improved graphitization and restoration of the conjugated carbon network.

This conclusion can also be verified by Raman spectra measurement (Figs. 1d). It can be seen two characteristic peaks of carbon materials corresponding to the D and G signals at 1 345 cm^{-1} and 1 592 cm^{-1}, respectively [28]. The G peak is usually used to characterize the sp^2-bonded carbon atoms, and the D peak is related to the carbon atoms oscillations with dangling bonds in plane terminations of disordered graphite. The intensity ratio of the two (I_D/I_G) decreases from 0.95 (GO) to 0.61(RGO) after laser irradiation, which means the removal of OCGs and recovery of C-C hybridization [29]. This decrease in ID/IG reflects the partial restoration of sp^2 domains, which is essential for enhancing electrical conductivity. The removal of hydrophilic OCGs further contributes to the conductivity recovery. A 2D peak at 2 704 cm^{-1} in the RGO spectra can also be observed, again indicating the effective reduction of GO film. In addition, the typical diffraction peak at 2θ = 11.05° in the XRD curve of GO material disappears with laser treatment (Figs. 1e), which is further consistent with the above conclusion well [30-31]. The OCGs on the surface of GO film have an adverse effect on its conductivity. Hence, the non-conductive part of GO naturally plays a role in isolating the interdigital electrodes, and the controllable conductivity of RGO is also crucial to ensuring the high performance of FS-MSC devices in the subsequent experiments.After analyzing the above-mentioned basic characteristics of the samples, we then tested the electrochemical performance and mechanical robustness. Due to the excellent physical flexibility, the electrode/polymer film can be assembled closely onto the attachments with different curvatures (Figs. 2a). The devices can maintain stability even under harsh conditions where they were bent by more than 300 degrees on a millimeter scale. To describe the performance in detail, we measured the typical electrochemical response curves and compared their changes under different bending conditions. The PVA-H_3PO_4 solid electrolyte was employed on the surface of interdigital electrode and a two-electrode system was applied here (detailed in SI S4).

Figs. 2b shows typical cyclic voltammetry (CV) curves of our device under scan rate of 20, 30, 40 and 100 mV/s, respectively. The specific capacitances (C_s) are calculated by the formula below:

$$C_S = \frac{\int_{V_L}^{V_H} IdV}{A \cdot S \cdot (V_H - V_L)} \quad , \qquad (1)$$

Where the I, S, A, V_H and V_L are current density, scan rate, electrode acreage, discharge start voltage and discharge end voltage, respectively. The initial C_s calculated from the CV curves, presented as a near-rectangular shape, at 10 mV/s scan rate is 0.86 mF/cm^2. With the increase of scan speed, the extracted capacitance decreases gradually, which can be also proven in the galvanostatic charge/discharge (GCD) results measured under different current density of 0.01, 0.015, 0.02 and 0.05 mA/cm^2, as shown in Figs. 2c [32-33]. The GCD curves are symmetrical and approximate to triangle, indicating that our device has good coulomb efficiency. Based on the discharge time (Δt), the C_s value can be calculated by the following formula:

$$C_S = \frac{I \cdot \Delta t}{A \cdot \Delta V} \quad , \qquad (2)$$

Where ΔV is the potential difference between

the start and end of the discharge. The corresponding initial C_s calculated from the GCD plot at 0.005 mA/cm^2 current density is 1.47 mF/cm^2. As the scan rate and the current density respectively increases (10 to 100 mV/s, 0.005 to 0.05 mA/cm^2), only 20% and 16% of the initial values remains (Figs. 2d), indicating limited rate performance. This is mainly due to the high viscosity of the PVA-H_3PO_4 gel electrolyte, which restricts ion migration at high current densities. At the same time, the stacked RGO sheets present relatively high interfacial impedance, which aggravate polarization. To address these issues, several improvement strategies can be explored in the subsequent experiments. For example, we fabricated the RGO/MnO_2 composite electrodes by adding MnO_2 to the GO precursor. The composite device showed a capacitance 5 times higher than that of the pure RGO device at 20 mV/s, and a capacitance retention of 38.5% when the current density increased from 0.05 to 0.1 mA/cm^2, indicating improved rate capability. A systematic investigation of composite electrodes is planned for future work (SI S5).

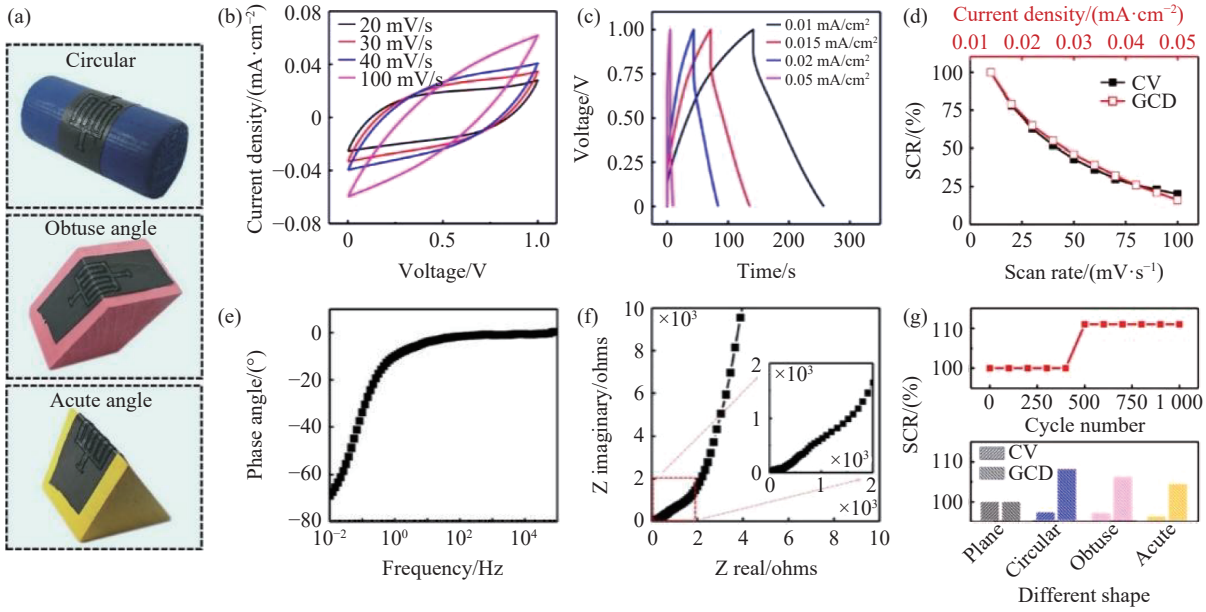

Fig. 2 (a) OM images of our RGO FS-MSCs assembled on the attachments with different curvatures. (b)-(c) CV and GCD curves respectively measured under different scan rates and current densities, (d)-(f) specific capacitance retention (SCR), variation on frequency, and Nyquist plots of the devices. (g) SCR of devices after 1 000 bending cycles (top) and the corresponding CV, GCD performance comparison at different bending conditions (bottom).

Furthermore, we also measured the frequency-dependent response of our devices with electrochemical impedance spectroscopy (EIS), reflected as Bode diagram in Figs. 2e [34]. The phase angle of the supercapacitor is about −70°, and the response time is calculated as short as 2.83 s. At the same time, the large slope of the curve in its low-frequency range (~225 degree/Hz). Moreover, in the high-frequency range, the Nyquist curve intersects the real part axis of the impedance at a point, corresponding to an internal resistance of about 33 Ω (Figs. 2f). It should be noted that the hydrogel used in our device will gradually lose water over time, and the corresponding ionic conductivity will decrease as a result, leading to the degradation of the device's performance. In the later stage, if we want to maintain the excellent performance of the device, we need to rehydrate the gel electrolyte appropriately. The detailed description can be found in SI S6.

After testing the typical electrochemical properties of our devices, we then focused on their per-

formance and bending stability next. Figs. 2g (top) shows their specific capacitance retention (SCR) results, and the capacitance remains above 111% of the initial values after 1 000 charge-discharge cycles. The sudden increase in capacitance after 400 cycles may be due to the improved wettability at the electrode-electrolyte interface and fuller electrochemical activation, which in turn favors the storage of higher electrochemical charges [35]. Similar phenomena have been observed in other RGO-based flexible supercapacitors. Figs. 2g (bottom) presents the CV and GCD performance comparison of the devices under different bending conditions. The CV and GCD results were measured at a scan rate of 20 mV/s and a current density of 0.01 mA/cm^2, respectively. Compared with the performance of our devices without deformation, the average variation of CV and GCD curves caused by bending are only about 3.5% and 6.8%. These almost identical tested results once again demonstrate an excellent bending robustness of the RGO FS-MSCs. In addition, we have also developed processing techniques for multi-device series and parallel connection. More detailed discussions have been shown in SI S7.

Furthermore, the stretchability of these devices was also tested and compared. We first set up the elastomeric substrate surface as a periodic grating structure and fit it to the polymer/RGO electrode film after pre-stretching it by 120% deformation. The tensile direction of the substrate is perpendicular to the one of the grating. The period of the grooves is ~1 mm with a duty factor of 3:7 and the depth is ~850 μm, as shown in a three-dimensional (3D) morphology image in Figs. 3a. This structural design of the devices enables them to maintain stable performance. A variation of <5.3% in CV and GCD curves can be guaranteed as the RGO electrode film is integrated with the structured substrate (Figs. 3b, SI S8). Then, the CV and GCD performance of the above devices under different tensile states were measured in detail. When the tensile strain increases from 0% to 120% gradually, the integral area of CV plots increases slightly with a kept scanning speed of 20 mV/s. The extracted Cs increases from 0.52 to 0.69 mF/cm^2, which is mainly because the electrode film flattens in a larger tension condition and the charges are more fully in contact with gel electrolyte at this time (Figs. 3c) [12,36]. Similar trends are also reflected in the GCD curves with a current density of 0.01 mA/cm^2 in Figs. 3d. However, when the scan rate and current density are respectively increased from 10 to 100 mV/s and 0.01 to 0.05 mA/cm^2, significant decreases in the SCR values to 12.4% and 13.4% can be clearly observed (Figs. 3e). But when we focus on the difference caused by the tensile strain under a certain measurement condition, we can found a performance fluctuation less than 7.8%, which also reflects the tensile stability of our devices from the side. The detailed measured CV and GCD curves can be seen in SI S9.

In addition, to more clarify the wearable of the RGO FS-MSCs, we tested the device by attaching it on the finger for bending measurement. GCD curves of RGO FS-MSCs at a current density of 0.02 mA/cm^2 have also been tested at bending degrees of 0°, 80° and 120°, respectively. All the GCD curves of RGO FS-MSCs with structured substrates (gridding in Fig.4) were almost retained equilateral triangle shape. Meanwhile, the GCD curves of the RGO FS-MSCs under 80° and 120° bending degree were well overlapped for the initial status. The capacitances are 0.52, 0.53 and 0.56 mF/cm^2, respectively. The above results indicate that our device still maintains performance stability in practical applications and can be used in real-world scenarios. More detailed information can be seen in SI S10.

It should be noted that the fluctuation in the electrochemical performance of the above-mentioned FS-MSCs during stretching may come from the uneven stress distribution caused by the single directional grating structures of the substrate [37]. For this reason, we further designed and fabricated the gridding that intersects vertically on the substrate by

using the laser processing technique. In contrast, the characteristic widths of the gridding pits were kept unchanged as 500 μm, while the spacing between them was adjusted to 200, 500 and 800 μm, respectively. The S5-2, S5-5 and S5-8 were used to conveniently distinguish these samples with different signatures. A 120% pre-stretching was also carried out along the direction of one edge of gridding before attaching them to the RGO electrode film. Nevertheless, due to the discrepancy in gridding spacing between different types of samples, there was a deformation deviation of about 2% when the same tensile strength was applied to achieve the 120% tensile strain. The specific morphologies of these samples have been shown in the optical images in Figs. 4a, 4b and SI S11.

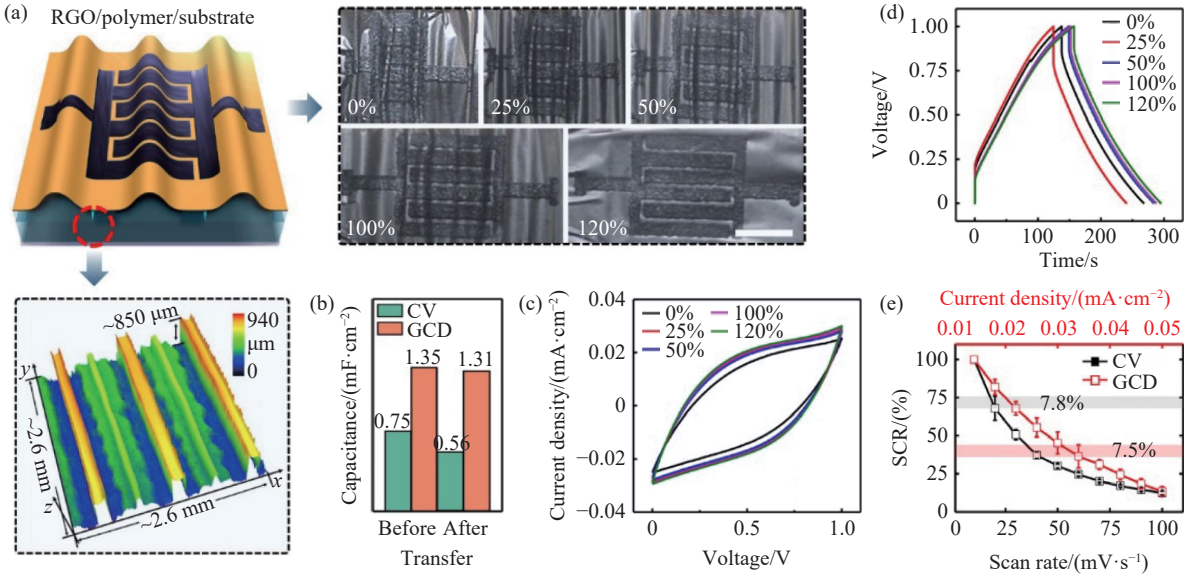

Fig. 3 (a) FS-MSC schematic (top), 3D confocal laser scanning microscopy (CLSM) image of the structured substrate (bottom), and the OM images of the FS-MSCs at different tensile strain conditions. The scale is 3 mm. The 120% of the tensile strain corresponds to a stretching deformation of 220% of the initial length of sample. Other tensile strain conditions are defined according to the same criteria. (b) Cs values comparison calculated from CV (scan rate 20 mV/s) and GCD (current density 0.01 mA/cm^2) curves before and after the RGO supercapacitor is transferred to an elastomeric substrate. (c)-(d) The CV (scan rate 20 mV/s) and GCD performance (current density 0.01 mA/cm^2) of the devices under different tension conditions. (e) SCR of the devices with the increase of scan rate and current density.

For devices based on the newly designed substrates, we repeated the previous electrochemical experiments. We first measured the CV and GCD curves of RGO FS-MSCs with the different substrates (S5-2, S5-5 and S5-8) under different stretching states. The scanning speed and the current density were also focused as 20 mV/s and 0.01 mA/cm^2, respectively. Through the performance comparison, we found that the sample S5-5 presented the largest integral area and longest discharge time, which directly indicates a highest capacitance with an optimal design of the substrate structure. Therefore, the change of its performance will be focused on as a representative in the follow-up work (SI S12 and Table S1). Owing to the stress regulation provided by the grids within the substrate, our device exhibits stable electrochemical performance under stretching along perpendicular in-plane directions. The CV curves measured at 50% and 120% stretching states almost overlap, indicating that the ionic conductivity and electrochemical stability of the gel electrolyte are well maintained during mechanical deformation. The detailed performance can be found in SI S13.

It is not difficult to find that the optimization of the substrate structure also plays a crucial role in

maintaining the stability of the device performance. We extracted flag values and compared them to more intuitively observe the fluctuation difference with previous groove-structured FS-MSCs. Fig. 4c shows the comparisons, suggesting more stable SCR in a gridding-structured FS-MSC (S5-5) during stretching. Both the specific capacitance value fluctuations got from the CV and GCD curves of the S5-5 FS-MSC are less than 5.6%. We further extracted the SCR under different tensile conditions. Although the rate performance of S5-5 FS-MSC decreased with the increase of scan rate and current density, the performance fluctuation caused by the stretching was still minimal (Fig. 4d, fluctuation calculated in Formula S1). To observe the difference more intuitively, we fixed the current density and extracted the specific capacitance of FS-MSCs with difference substrates (Table S1). As the tensile strain changes from 0% to 120%, most of the capacitance values show a trend of improvement. The overall performance of our devices is most efficient when the surface is flattened. Both the electrochemical performance and mechanical robustness are significantly improved when the substrate structures are optimized as S5-5 FS-MSC architectures. The maximum capacitance is 1.34 mF/cm^2 with 1.5% fluctuation (current density: 0.01 mA/cm^2) at different tensile states. Even the current density gradually increased from 0.01 to 0.05 mA/cm^2, above 92.6% of specific capacitance fluctuation stability could be still remained (Formula S2). Thanks to the simple laser processing strategy, device pre-stretching technique, and the stress regulation by micro/nanostructured substrates, our devices exhibit excellent electrochemical performance and stability. Table 1 presents a performance comparison between representative laser-treated MSCs and our devices.

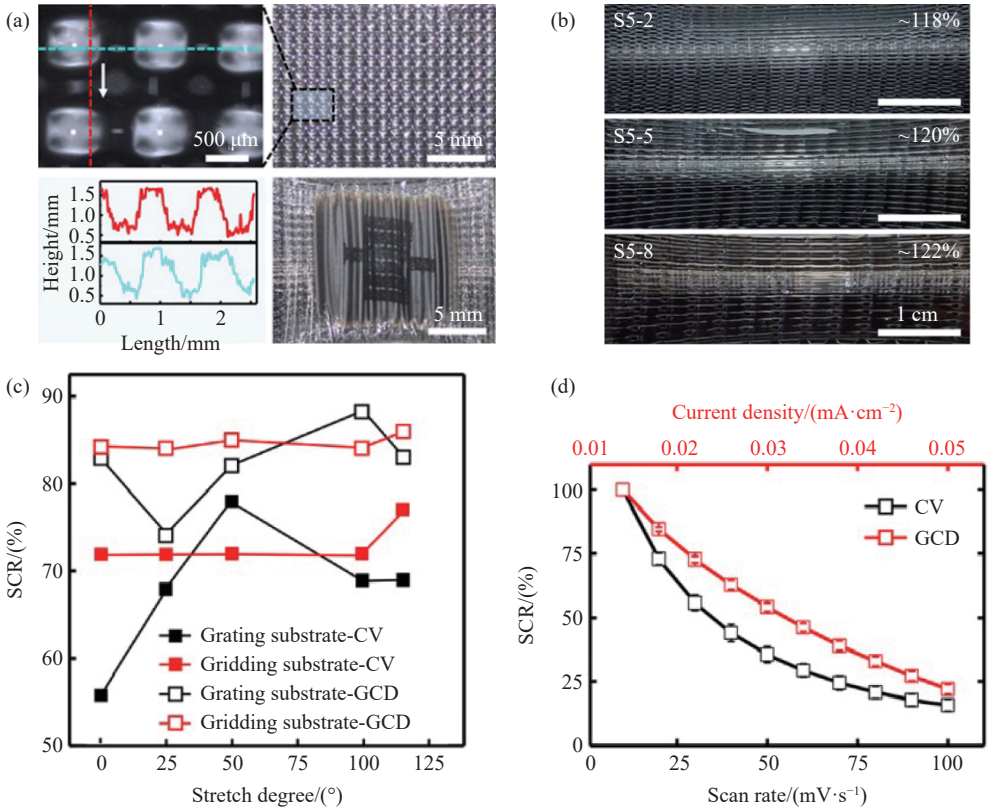

Fig. 4 (a) OMs of the gridding substrate and the corresponding assembled RGO FS-MSC. (b) OMs of the S5-2, S5-5 and S5-8 substrates under pre-stretching. (c) SCR comparison of RGO FS-MSCs assembled on the groove and gridding substrates under different tensile conditions. (d) SCR comparison of S5-5 FS-MSC. The numerical errors are caused by the difference in tensile strength.

Tab. 1 Performance comparison between laser-processed graphene-based supercapacitors

Laser	Wavelength (nm)	Material	Areal Capacitance (mF/cm^2)	Flexibility	Stretchability	Stability	Reference
UV	346	GO/leaves	34.68	99% retention (0–60°)	–	99%@50k cycles 100%@20k (45°)	[38]
	355	GO-MG-(PANI)/PET/PI/PTFE	3.8	F	–	82%@20k cycles 86%@1k (150°)	[39]
	355	GO/SEBS	1.336	98% retention (0–180°)	20%	90%@1k bend 90%@1k (20%)	[40]
	355	CNT/ natural latex balloon	13.5	F	400%	93%@12k cycles 97%@200 (20%)	[9]
VIS	400-450	FB-LIG/PI	49.81	99% retention (0–180°)	–	97.56%@10k cycles 90.16%@10k (90°)	[41]
	405	Mxene-GO/PET	2.58	98% retention (0–150°)	–	97.7%@10k cycles	[42]
	405	PEDOT-GO/PET	5.78	98% retention (0–135°)	–	85.4%@5k cycles	[43]
NIR	800	GO-MnO_2	128	F	–	95%@12k cycles 100%@0–180° bend	[44]
	1 030	GO/PET	7.2 F/cm^3	95% retention (0–180°)	–	96%@10k cycles	[45]
	1 030	GO-RuO_2/ PET	2.35	F	–	90%@4k cycles	[46]
	1 064	GO/PVA	88.32	95% retention (0–180°)	–	82%@2k cycles 95%@5k (90°)	[47]
MIR	10 600	GO	3.41	F	–	99%@1k cycles (1%)	[48]
	10 600	GO/PET	43.7	F	–	90%@3k cycles	[49]
	10 600	LIG-CrO_x/PI	13.48	99% retention (0–90°)	–	85%@1.5k cycles	[50]
	10 600	NiO-Co_3O_4-GO/WPU	2.4	100% retention (±180°)	280%	98.4%@10k 80.2%@1k (100%)	[51]
	10 600	GO/3M tape	1.34	96.5% retention (>300°)	120%	111%@1k (>300°)	This work

4 Conclusion

In summary, we have demonstrated a single-laser, dual-function programmable processing strategy for RGO flexible/stretchable FS-MSCs. By photoreduction and photoetching using a single laser source, the electrochemical electrodes and structured substrates of the device can be prepared simultaneously, simplifying the procedure of device fabrication significantly. By integrating the electrodes with substrate under pre-stretching, devices with bending angle of >300° and a tensile strain of ~120% can be achieved. The reactive activation and large specific surface area of electrodes ensure the outstanding electrochemical performance, and the uniform stress distribution on the substrate with optimized gridding structures can effectively improve the stability. The maximum capacitance of 1.34 mF/cm^2 and 1.5% fluctuation at different tensile strain conditions are observed. This work offers a practical, open-ended design paradigm for high-stability wearable energy storage devices, with clear pathways to further enhance rate capability, such as electrolyte modification, electrode thinning, porosity engineering, or the use of composite materials.

References:

[1] TAMANG S, RAI S, BHUJEL R, *et al*.. A concise review on GO, rGO and metal oxide/rGO composites: fabrication and their supercapacitor and catalytic applications[J]. *Journal of Alloys and Compounds*, 2023, 947: 169588.

[2] ZHANG P P, WANG F X, YU M H, *et al*.. Two-dimensional materials for miniaturized energy storage devices: from individual devices to smart integrated systems[J]. *Chemical Society Reviews*, 2018, 47(19): 7426-7451.

[3] WANG S L, LIU N SH, SU J, *et al*.. Highly stretchable and self-healable supercapacitor with reduced graphene oxide based fiber springs[J]. *ACS Nano*, 2017, 11(2): 2066-2074.

[4] KUMAR R, JOANNI E, SAHOO S, *et al*.. An overview of recent progress in nanostructured carbon-based supercapacitor electrodes: from zero to bi-dimensional materials[J]. *Carbon*, 2022, 193: 298-338.

[5] KIM K W, PARK S J, PARK S J, *et al*.. Deformable micro-supercapacitor fabricated via laser ablation patterning of Graphene/liquid metal[J]. *npj Flexible Electronics*, 2024, 8(1): 18.

[6] YANG ZH B, DENG J, CHEN X L, *et al*.. A highly stretchable, fiber-shaped supercapacitor[J]. *Angewandte Chemie International Edition*, 2013, 52(50): 13453-13457.

[7] SUN J F, HUANG Y, FU CH X, *et al*.. High-performance stretchable yarn supercapacitor based on PPy@CNTs@urethane elastic fiber core spun yarn[J]. *Nano Energy*, 2016, 27: 230-237.

[8] XIAO H, WU ZH SH, CHEN L, *et al*.. One-step device fabrication of phosphorene and graphene interdigital micro-supercapacitors with high energy density[J]. *ACS Nano*, 2017, 11(7): 7284-7292.

[9] WANG Y, ZHAO Y, HAN Y Y, *et al*.. Fixture-free omnidirectional prestretching fabrication and integration of crumpled in-plane micro-supercapacitors[J]. *Science Advances*, 2022, 8(21): eabn8338.

[10] KALTENBRUNNER M, SEKITANI T, REEDER J, *et al*.. An ultra-lightweight design for imperceptible plastic electronics[J]. *Nature*, 2013, 499(7459): 458-463.

[11] WANG Y, LIU W W, XIN W, *et al*.. Back-reflected performance-enhanced flexible perovskite photodetectors through substrate texturing with femtosecond laser[J]. *ACS Applied Materials & Interfaces*, 2020, 12(23): 26614-26623.

[12] ZUO J Y, HAN D X, YAO H F, *et al*.. Stretching the future: strategies and emerging trends in stretchable organic photovoltaic materials[J]. *Energy & Environmental Science*, 2025, 18(13): 6344-6365.

[13] ENRICO A, BUCHMANN S, DE FERRARI F, *et al*.. Cleanroom - free direct laser micropatterning of polymers for organic electrochemical transistors in logic circuits and glucose biosensors[J]. *Advanced Science*, 2024, 11(27) : 2307042.

[14] KALRA A, LOWE A, AL-JUMAILY A M. Mechanical behaviour of skin: a review[J]. *Journal of Material Science & Engineering*, 2016, 5(4): 1000254.

[15] AGACHE P G, MONNEUR C, LEVEQUE J L, *et al*.. Mechanical properties and Young's modulus of human skin in vivo[J]. *Archives of Dermatological Research*, 1980, 269(3): 221-232.

[16] JIANG H B, LIU Y Q, ZHANG Y L, *et al*.. Reed leaf-inspired graphene films with anisotropic superhydrophobicity[J]. *ACS Applied Materials & Interfaces*, 2018, 10(21): 18416-18425.

[17] ZOU T T, ZHAO B, XIN W, *et al*.. High-speed femtosecond laser plasmonic lithography and reduction of graphene oxide for anisotropic photoresponse[J]. *Light: Science & Applications*, 2020, 9(1): 69.

[18] ZOU T T, ZHAO B, XIN W, *et al*.. Birefringent response of graphene oxide film structurized via femtosecond laser[J]. *Nano Research*, 2022, 15(5): 4490-4499.

[19] KUMAR R, SAHOO S, JOANNI E, *et al*.. Recent progress in the synthesis of graphene and derived materials for next generation electrodes of high performance lithium ion batteries[J]. *Progress in Energy and Combustion Science*, 2019, 75: 100786.

[20] KERSE C, KALAYCIOĞLU H, ELAHI P, *et al*.. Ablation-cooled material removal with ultrafast bursts of pulses[J]. *Nature*, 2016, 537(7618): 84-88.

[21] ZHAI T R, ZHANG X P, PANG ZH G, *et al*.. Direct writing of polymer lasers using interference ablation[J]. *Advanced Materials*, 2011, 23(16): 1860-1864.

[22] AHMAD Z, CABRAL J T. Navigating the labyrinth of isotropic wrinkling: design, fabrication, characterization, and applications[J]. *Materials Horizons*, 2026, 13(8): 3658-3696.

[23] ZHAO CH, JIA X T, SHU K W, *et al*.. Stretchability enhancement of buckled polypyrrole electrodes for stretchable supercapacitors via engineering substrate surface roughness[J]. *Electrochimica Acta*, 2020, 343: 136099.

[24] GUO L, ZHANG Y L, HAN D D, *et al*.. Laser-mediated programmable N doping and simultaneous reduction of graphene oxides[J]. *Advanced Optical Materials*, 2014, 2(2): 120-125.

[25] GUAN Y CH, DING Y, FANG Y Q, *et al*.. Far-field femtosecond laser-driven λ/73 super-resolution fabrication of 2D van der Waals $NbOI_2$ nanostructures in ambient air[J]. *Nature Communications*, 2025, 16(1): 4149.

[26] JIANG H B, ZHANG Y L, HAN D D, *et al*.. Bioinspired fabrication of superhydrophobic graphene films by two-beam laser interference[J]. *Advanced Functional Materials*, 2014, 24(29): 4595-4602.

[27] FU X Y, ZHANG Y L, JIANG H B, *et al*.. Hierarchically structuring and synchronous photoreduction of graphene oxide

films by laser holography for supercapacitors[J]. *Optics Letters*, 2019, 44(7): 1714-1717.

[28] FANG X X, HU F, LU J J, *et al*.. Laser-induced graphene as an effective supporting structure for high performance Ge anode applied in Li-ion batteries[J]. *Journal of Colloid and Interface Science*, 2025, 688: 656-663.

[29] HAN D D, ZHANG Y L, MA J N, *et al*.. Sunlight-reduced graphene oxides as sensitive moisture sensors for smart device design[J]. *Advanced Materials Technologies*, 2017, 2(8): 1700045.

[30] XU X J, LIN H CH, DING J R, *et al*.. NiCoMn-LDH with core-shell heterostructures based on CoS nanotube arrays containing multiple ion diffusion channels for boosted supercapacitor applications[J]. *Green Energy & Environment*, 2025, 10(4): 780-792.

[31] HAN D D, ZHANG Y L, JIANG H B, *et al*.. Moisture-responsive graphene paper prepared by self-controlled photoreduction[J]. *Advanced Materials*, 2015, 27(2): 332-338.

[32] SHABANI SHAYEH J, EHSANI A, GANJALI M R, *et al*.. Conductive polymer/reduced graphene oxide/Au nano particles as efficient composite materials in electrochemical supercapacitors[J]. *Applied Surface Science*, 2015, 353: 594-599.

[33] CHEN J CH, WANG Y M, CAO J Y, *et al*.. Facile Co-electrodeposition method for high-performance supercapacitor based on reduced graphene oxide/polypyrrole composite film[J]. *ACS Applied Materials & Interfaces*, 2017, 9(23): 19831-19842.

[34] ZANG X B, XU R Q, ZHANG Y Y, *et al*.. All carbon coaxial supercapacitors based on hollow carbon nanotube sleeve structure[J]. *Nanotechnology*, 2015, 26(4): 045401.

[35] FU X Y, ZHANG Y Y, MA CH J, *et al*.. Programmable patterning fabrication of laser-induced graphene-MXene composite electrodes for flexible planar supercapacitors[J]. *Optics Letters*, 2022, 47(6): 1502-1505.

[36] NIU ZH Q, DONG H B, ZHU B W, *et al*.. Highly stretchable, integrated supercapacitors based on single-walled carbon nanotube films with continuous reticulate architecture[J]. *Advanced Materials*, 2013, 25(7): 1058-1064.

[37] LV ZH SH, LUO Y F, TANG Y X, *et al*.. Editable supercapacitors with customizable stretchability based on mechanically strengthened ultralong MnO_2 nanowire composite[J]. *Advanced Materials*, 2018, 30(2): 1704531.

[38] LE T S D, LEE Y A, NAM H K, *et al*.. Green flexible graphene–inorganic-hybrid micro - supercapacitors made of fallen leaves enabled by ultrafast laser pulses[J]. *Advanced Functional Materials*, 2022, 32(20): 2107768.

[39] YE J L, TAN H B, WU SH L, *et al*.. Direct laser writing of graphene made from chemical vapor deposition for flexible, integratable micro-supercapacitors with ultrahigh power output[J]. *Advanced Materials*, 2018, 30(21): 1801384.

[40] KIM K W, PARK S J, PARK S J, *et al*.. Deformable micro-supercapacitor fabricated via laser ablation patterning of graphene/liquid metal[J]. *npj Flexible Electronics*, 2024, 8(1): 18.

[41] YUAN G Y, WAN T, BAQAIS A, *et al*.. Boron and fluorine Co-doped laser-induced graphene towards high-performance micro-supercapacitors[J]. *Carbon*, 2023, 212: 118101.

[42] ZHU Y Y, NI ZH Y, GAO J, *et al*.. Fabrication of flexible planar micro-supercapacitors using laser scribed graphene electrodes incorporated with MXene[J]. *Journal of Physics and Chemistry of Solids*, 2023, 183: 111619.

[43] HU H W, GUO Y Y, ZHAO J. Manufacturing shape-controllable flexible PEDOT/rGO composite electrodes for planar micro-supercapacitors[J]. *Materials*, 2024, 17(9): 2144.

[44] YUAN Y J, JIANG L, LI X, *et al*.. Laser photonic-reduction stamping for graphene-based micro-supercapacitors ultrafast fabrication[J]. *Nature Communications*, 2020, 11(1): 6185.

[45] LI Q, DING Y, YANG L J, *et al*.. Periodic nanopatterning and reduction of graphene oxide by femtosecond laser to construct high-performance micro-supercapacitors[J]. *Carbon*, 2021, 172: 144-153.

[46] WANG L F, DING Y, LI J Y, *et al*.. Femtosecond laser induced one-step nanopatterning and preparation of rGO/RuO_2 electrodes for high-performance micro-supercapacitors[J]. *Journal of Electroanalytical Chemistry*, 2022, 919: 116501.

[47] ZHAO Y R, DU J W, DU J J, *et al*.. Realizing highly - ordered laser - reduced graphene for high - performance flexible microsupercapacitor[J]. *Small*, 2023, 19(35): 2301546.

[48] WANG Y N, WANG Y, ZHANG P P, *et al*.. Laser - induced freestanding graphene papers: a new route of scalable fabrication with tunable morphologies and properties for multifunctional devices and structures[J]. *Small*, 2018, 14(36): 1802350.

[49] KWON S, YOON Y, AHN J, *et al*.. Facile laser fabrication of high quality graphene-based microsupercapacitors with large capacitance[J]. *Carbon*, 2018, 137: 136-145.

[50] YANG J, ZHENG Y Y, LIU W J, *et al*.. MOF-derived graphene/chromium oxide hybrids via laser processing for enhanced planar micro-supercapacitors[J]. *Applied Physics Letters*, 2026, 128(1): 013904.

[51] WANG W T, LU L SH, XIE Y X, *et al*.. A highly stretchable microsupercapacitor using laser-induced graphene/NiO/Co_3O_4 electrodes on a biodegradable waterborne polyurethane substrate[J]. *Advanced Materials Technologies*, 2020, 5(2): 1900903.

Author Biographies:

JIANG Hao-bo (1988—) is a associate professor and master's supervisor from Changchun, Jilin Province. She received her Ph.D. in 2016 from the college of Electronic Science and Engineering at Jilin University. Her current research focuses on laser micro/nano fabrication of two-dimensional materials, for example, graphene, and their applications in energy storage devices. E-mail: jianghaobo@jlnu.edu.cn

姜昊伯(1988—), 女, 吉林长春人, 博士, 副教授, 硕士研究生导师, 2016 年于吉林大学电子科学与工程学院获得博士学位, 主要从事石墨烯等二维材料的激光微纳制造与储能器件的研究。 E-mail: jianghaobo@jlnu.edu.cn

XIN Wei (1987—) is a associate professor and doctoral supervisor from Tonghua, Jilin Province. He received his Ph.D. from Nankai University in 2017. He then worked and studied at several institutions, including the Changchun Institute of Optics, Fine Mechanics and Physics, Zhejiang University, and the Shanghai Institute of Technical Physics. His current research focuses on the micro/nano optoelectronic properties of two-dimensional materials and their device performance. E-mail: xinwei@nenu.edu.cn

辛巍(1987—), 男, 吉林通化人, 博士, 副教授, 博士研究生导师。2017 年于南开大学获得博士学位, 后分别在中国科学院长春光学精密机械与物理研究所、浙江大学、中国科学院上海技术物理研究所等单位开展学习与研究工作, 主要从事二维材料微纳光电原理探索与器件性能研究。E-mail: xinwei@nenu.edu.cn

FU Xiu-yan (1991—) is a lecturer and master's supervisor from Taian, Shandong Province. She received her Ph.D. from Jilin University in 2020. Her research primarily focuses on laser processing of two-dimensional nanomaterials for energy storage devices. E-mail: fuxy@jlnu.edu.cn

付秀燕(1991—), 女, 山东泰安人, 博士, 讲师, 硕士研究生导师, 2020 年于吉林大学获得博士学位, 主要从事激光加工二维纳米材料储能器件的研究。E-mail: fuxy@jlnu.edu.cn